PROCEEDINGS OF SCIENCE

ONLINE ICRC 2021
THE ASTROPARTICLE PHYSICS CONFERENCE
Berlin | Germany
37th International Cosmic Ray Conference
12–23 July 2021

Particle acceleration in supernova remnant expanding inside wind-blown bubble

Samata Das,[a,b,*] **Robert Brose,**[c] **Dominique M.-A. Meyer,**[b] **Martin Pohl,**[a,b] **Iurii Sushch**[d,e] **and Pavlo Plotko**[a]

[a] *DESY, Platanenallee 6, Zeuthen D-15738 , Germany*
[b] *University of Potsdam, Institute of Physics and Astronomy, Karl-Liebknecht-Strasse 24/25, Potsdam 14476, Germany*
[c] *Dublin Institute for Advanced Studies, 31 Fitzwilliam Place, Dublin 2, Ireland*
[d] *North-West University, Centre for Space Research, Potchefstroom 2520, South Africa*
[e] *Astronomical Observatory of Ivan Franko National University of L'viv, vul. Kyryla i Methodia 8, L'viv 79005, Ukraine*
E-mail: samata.das@desy.de, robert.brose@desy.de, domimeyer@uni-potsdam.de, marpohl@uni-potsdam.de, iurii.sushch@desy.de, pavlo.plotko@desy.de

Context. Supernova Remnants (SNRs) are considered as the primary sources of galactic cosmic rays (CRs), where CRs are assumed to be accelerated by diffusive shock acceleration (DSA) mechanism. The SNR shocks expand in the complex ambient environment, particularly in the core-collapse scenarios as those SNRs evolve inside wind-blown bubbles created by the mass-loss of massive stars. Therefore, the evolution of core-collapse SNRs, as well as CRs acceleration is expected to be considerably different from SNR evolution in a uniform environment.

Aims. The aim is to observe the influence of different ambient medium of core-collapse SNR shock on the particle spectra. Furthermore, the interactions of SNR shock with fluctuations in density within the wind-blown bubble generate several transmitted and reflected shocks. So, the impact of SNR shock interactions with different discontinuities, on particle spectra, and finally the effect on emission from the remnant are also the areas of focus.

Methods. The hydrodynamic structures of wind-blown bubbles at pre-supernova stages formed by $20M_{\odot}$, $35M_{\odot}$, and $60M_{\odot}$ stars have been used to create the ambient environment for SNRs. Evolution of those stars through different stages from Zero Age Main Sequence (ZAMS) to the pre-supernova stage, results into formation of structurally different wind bubbles. Then, the transport equation for cosmic rays, and hydrodynamic equations have been solved simultaneously in 1-D spherical symmetry.

Result. The modifications in particle spectra depend on the hydrodynamics and magnetic field structure of SNR ambient medium. We have obtained softer spectra with spectra index close to 2.5 originated during SNR interaction with hot wind bubble and further, magnetic field structure effectively influences the emission morphology of SNR as it governs the transportation of particles.

37th International Cosmic Ray Conference (ICRC 2021)
July 12th – 23rd, 2021
Online – Berlin, Germany

*Presenter

PoS(ICRC2021)988

1. Introduction

Supernova Remnants (SNRs) are regarded as the major sources of galactic cosmic rays (CRs) below the knee energy ($\approx 10^{15}$ eV). The diffusive Shock Acceleration (DSA) process at SNR shock predicts that spectra of particles should follow a power-law in energy with the spectral index 2. But most of the observed SNRs data for instance IC443, Cas A, SN 1006, and W44 indicate considerable softening (softer than the spectral index $(s) = 2$) in particle spectra. This spectral modification can be explained theoretically with different approaches, for instance by diffusive shock re-acceleration of galactic CRs at the slow shock [1], the re-acceleration in fast-mode turbulence downstream of the forward shock [2] as well as the fall off in particle confinement in the vicinity of SNR shock because of the attenuation or weak driving of Alfvén waves [3, 4].

Further, the acceleration of CRs at shock depends on the structure of the ambient environment specifically in core-collapse scenario. The core-collapse SNR interacts with a complex circumstellar medium (CSM) while evolving inside the hot wind bubble, created by the winds of massive star and these interactions affect the particle acceleration at SNR shock. In this context, our aim is to highlight the possibility of spectral modification as well as softening in the core-collapse scenario. We have investigated the following questions regarding spectral modification:

- How do the hydrodynamics of CSM affect the particle spectra and emission?
- What are the effects of CSM magnetic field on particle spectra and emission?

2. Modeling

The diffusive shock acceleration at SNR forward shock has been modeled in test-particle approximation using RATPaC (Radiation Acceleration Transport Parallel Code) [7, 8].

2.1 Hydrodynamics

- **Construction of CSM at pre-supernova stage**: The interaction between the stellar winds with the ambient interstellar medium (ISM) and the modified morphology of CSM during the entire lifetime of a massive progenitor star has been modeled by applying the PLUTO code [12] for hydrodynamic simulation in 1-D spherical symmetry. The stellar wind properties have been obtained from pre-calculated stellar evolutionary tracks [5, 6].
- **Introducing supernova explosion**: A supernova explosion has been introduced through insertion of supernova ejecta in the pre-supernova stage CSM.

To study the evolution of the SNR inside the CSM, standard hydrodynamic equations

$$\frac{\partial}{\partial t}\begin{pmatrix}\rho\\ \vec{m}\\ E\end{pmatrix} + \nabla\begin{pmatrix}\rho\vec{u}\\ \vec{m}\vec{u} + p\vec{I}\\ (E+p)\vec{u}\end{pmatrix}^{T} = \begin{pmatrix}0\\0\\0\end{pmatrix} \tag{1}$$

have been solved in 1-D spherical symmetry using the PLUTO code, where ρ, $\vec{u}$, $\vec{m}$, p, E are fluid density, velocity, momentum density, thermal pressure, and the total energy density with adiabatic index $5/3$ respectively, $\vec{I}$ is the unit tensor.

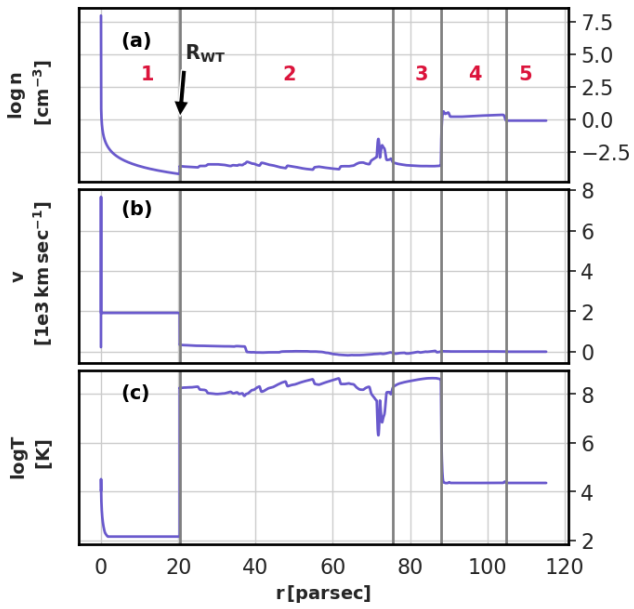

Figure 1: Hydrodynamic parameters after the supernova explosion for a non-rotating 60M$_\odot$ progenitor star with solar metallicity: number density n (panel (a)), flow velocity v (panel (b)), and temperature T (panel (c)). Vertical grey lines separate the Supernova ejecta (up to 0.023 parsec) and the free stellar wind (region 1), the shocked Luminous Blue Variable (LBV) and Wolf Rayet (WR) wind (region2), the shocked wind from O and B phases (region 3), the shocked interstellar medium (ISM) (region 4), and the ambient ISM (region 5). The density jump at the transition of region 1 and region 2, and region 3 and region 4 are the position of wind termination shock (R_{WT}), and the contact discontinuity respectively.

2.2 Magnetic Field

Two different prescriptions have been considered to construct the magnetic field structure:

- **Constant compressed Magnetic Field** (B_{const}): A simple magnetic field configuration, considering a strong magnetic field amplification in the shock precursor with a highly disordered upstream magnetic field, the downstream magnetic field (B_d) can be expressed in terms of upstream magnetic field (B_u) as [9],

$$B_d = r_B B_u \qquad r_B = \sqrt{(1 + 2R_{sub}^2)/3} \tag{2}$$

  where sub-shock compression ratio $R_{sub} = 4$ and $B_u = 5\mu G$.

- **Transported Magnetic Field** (B_{tran}): CSM magnetic field has been parametrised analytically on the basis of theoretical models and is transported through the forward shock (FS) to the downstream region. The subsequent evolution corresponds to MHD with negligible magnetic pressure. The magnetic field inside the CSM shaped by the $60M_\odot$ star, that becomes a WR star at pre-supernova stage, can be written as,

$$B_{CSM} = \begin{cases} (0.33\ \mu\text{G})\frac{R_{WT}}{r} & \text{region 1, beyond 0.023 parsec} \\ 1.32\ \mu\text{G} & \text{regions 2 \& 3} \\ 15.6\ \mu\text{G}, & \text{region 4} \\ 4.5\ \mu\text{G} & \text{region 5} \end{cases} \tag{3}$$

  where magnetic field in free wind region results from the Parker spiral for the toroidal magnetic field [11]. Additionally, the supernova ejecta magnetic field, $B_{ej}(r) \propto 1/r^2$. Then, the induction equation for ideal MHD has been solved [8] in 1-D spherical symmetry to obtain the evolution of the frozen-in magnetic field.

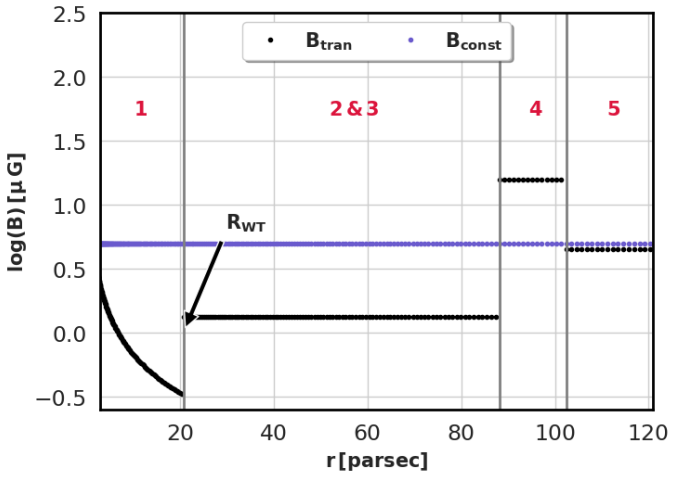

Figure 2: CSM magnetic field structures with two different configurations: $B_{\rm const}$, and $B_{\rm tran}$. Here, Region 1 only includes free stellar wind.

2.3 Particle acceleration

The time-dependent transport equation for the differential number density, N, of CRs

$$\frac{\partial N}{\partial t} = \nabla(D_{\rm r}\nabla N - \overrightarrow{u}N) - \frac{\partial}{\partial p}\left(\dot{p}N - \frac{\nabla.\overrightarrow{u}}{3}Np\right) + Q \tag{4}$$

have been solved in 1-D spherical symmetry in a shock-centred co-ordinate system considering only DSA at the FS in test-particle limit, where $D_{\rm r}$ is the spatial diffusion coefficient (10 times Bohm diffusion coefficient in the FS downstream and galactic diffusion coefficient in further FS upstream in our simulation), $\dot{p}$ corresponds to energy loss rate (synchrotron losses for electrons). $\overrightarrow{u}$ and Q refer to the plasma velocity and the source term, respectively. The source term is defined as [10],

$$Q = \eta n_{\rm u}(V_{\rm sh} - V_{\rm u})\delta(R - R_{\rm sh})\delta(p - p_{\rm inj}) \tag{5}$$

where η is the injection efficiency, $n_{\rm u}$ and $V_{\rm u}$ are the upstream plasma number density and velocity, respectively, $V_{\rm sh}$ and $R_{\rm sh}$ are shock velocity and radius, respectively, and $p_{\rm inj}$ represents the momentum of injected particles.

$$p_{\rm inj} = \xi p_{\rm th} = \xi\sqrt{2mk_BT_d}, \qquad \eta = \frac{4}{3\pi^{1/2}}(R_{\rm sub} - 1)\xi^3\exp(-\xi^2) \tag{6}$$

where $p_{\rm th}$ is the thermal momentum at the thermal peak of the Maxwell distribution of the downstream plasma with temperature $T_{\rm d}$.
The equations for the hydrodynamic evolution of SNR, the evolution of the large-scale magnetic field, and the CR transport equation have been solved in parallel using RATPaC.

2.4 Results

Shock Parameters: Applying the described numerical modeling, the evolution of SNR with $60M_\odot$ progenitor star has been studied for 45,000 years. The left panel of Figure 3 illustrates the time evolution of the position, velocity, and compression ratio of the FS. The shock velocity decreases sharply when the shock transits from free wind region to the denser shocked wind. It increases again after roughly 4800 years when another shock merges with the FS. Later, a lot of

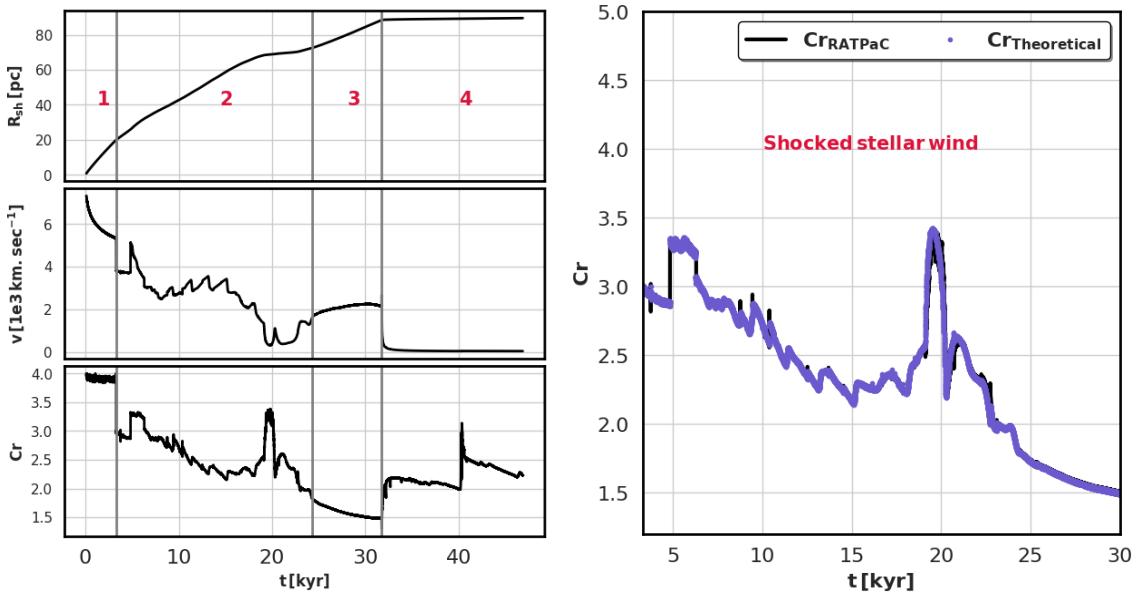

Figure 3: The left panel shows the behavior of the shock radius (R_{sh}), shock speed (v), and compression ratio (Cr) during evolution through different regions of the wind bubble. The right panel compares compression ratios: the numerical compression ratio, $Cr_{RATPaC} = v_u/v_d$ with v_u and v_d as the upstream and downstream flow speed in the FS rest frame, to the theoretical value, $Cr_{Theoretical} = ((1+\gamma)M_s^2)/((\gamma-1)M_s^2+2)$, where $\gamma = 5/3$ and M_s is the sonic Mach number in the FS rest frame.

fluctuations are visible in the shock velocity resulting from the interactions of FS with different discontinuities in the shocked wind zone. Finally, after 30,000 years the shock velocity decreases to almost 46 km. sec^{-1} when the FS collides with the contact discontinuity between region 3 and region 4 in Figure 1.

As soon as the FS enters into the shocked wind region, the compression ratio starts diverging from the value 4. The reason is that, the shocked wind region is very hot (shown in the panel (c) of Figure 1) and the FS turns into a shock with small sonic Mach number which immediately changes the value of compression ratio (shown in the right panel of Figure 2).

Particle Spectra: Proton (Pr) and electron (El) spectra show different spectral features during the evolution of FS in the different parts of CSM depending on the magnetic field. Figure 4 illustrates the Pr and El spectra at different ages with different magnetic field configurations depicted in Figure 2. At 2900 year, the spectra for Pr and El follow almost a p^{-2} power law when the FS is in the free wind region. In this region, magnetic field for $B_{\rm const}$ exceeds which provides higher maximum achievable energies for Pr and El than for $B_{\rm tran}$. After 5500 year, the softening in the spectra appears when FS is located in shocked wind, and additionally, in $B_{\rm tran}$ scenario, the spectra above 10 GeV become softer and cut off earlier than those from the less realistic simulation with $B_{\rm const}$. The reason behind this spectral modification above 10 GeV with $B_{\rm tran}$ is connected to the rise in the magnetic field strength at wind termination shock by a factor of 4. The high energy particles can reach the free wind region where the field strength is lower but particles with the lower energy ones only experience the magnetic field for region 2 & 3 in Figure 2. This can cause the spectral break near 10 GeV whereas in the $B_{\rm const}$ scenario, as we have considered constant magnetic field ($\approx 16.5\mu G$)

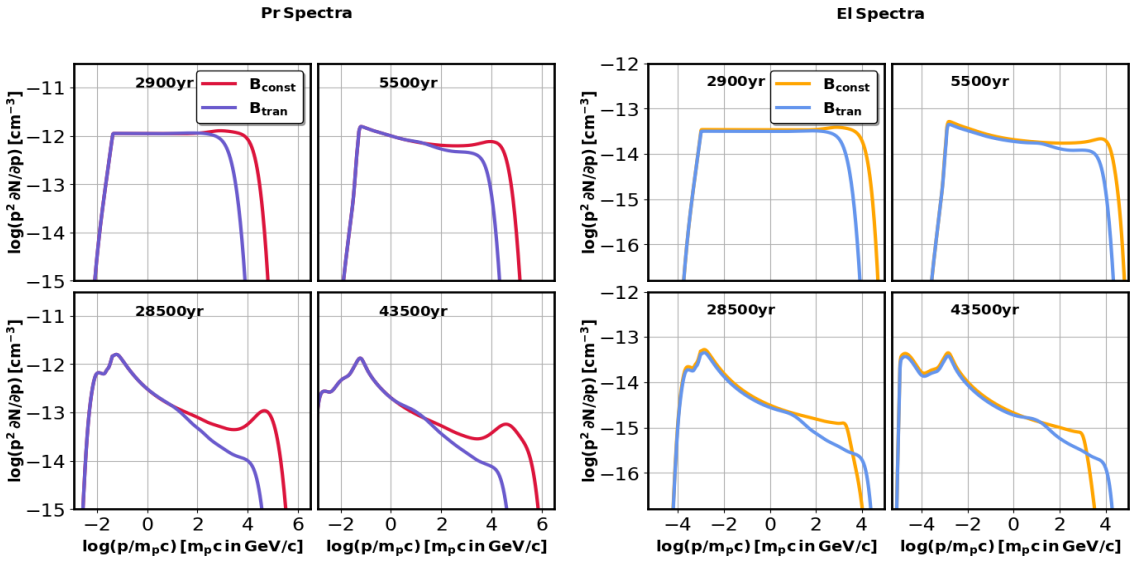

Figure 4: Proton (Pr) and Electron (El) spectra at different ages while SNR forward shock is in different regions of the wind bubble. We have averaged over the entire region downstream of the FS and distinguish constant compressed magnetic field (B_{cons}) and transported magnetic field (B_{tran}). Here, m_p is proton mass.

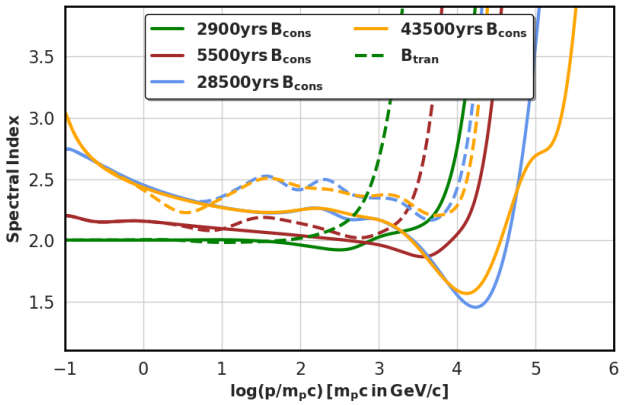

Figure 5: Variation with momentum of the spectral index for protons at different ages of SNR. The dashed line refer to models with transported magnetic field.

in the entire downstream, particles with any energy would experience same field strength. Then, at 28500 year, the FS already reaches the shocked wind from O and B phases, and the spectra become softer with time. Further, the maximum achievable energy of electrons for B_{tran} is higher, on account of the weak energy losses in the lower magnetic field, compared to B_{const}. Finally, the FS is in the dense shocked ISM at 43500 year, and the injection of low-energy particles is visible in the spectra. Additionally, with B_{const}, spectral hardening after almost 10^4GeV in proton spectra has been noticed and the spectral shape shows resemblance with non-linear DSA predicted spectra. However, the hardness reflects the pile-up of re-energized particles at the innermost reflected shock and stronger magnetic field in B_{const} scenario, emphasizes this effect. According to the obtained particle spectra, we can presume that in the core-collapse scenario, the spectra strongly diverge from the standard DSA prediction.

Non-thermal emission: We have calculated intensity maps of inverse Compton (IC) radiation and

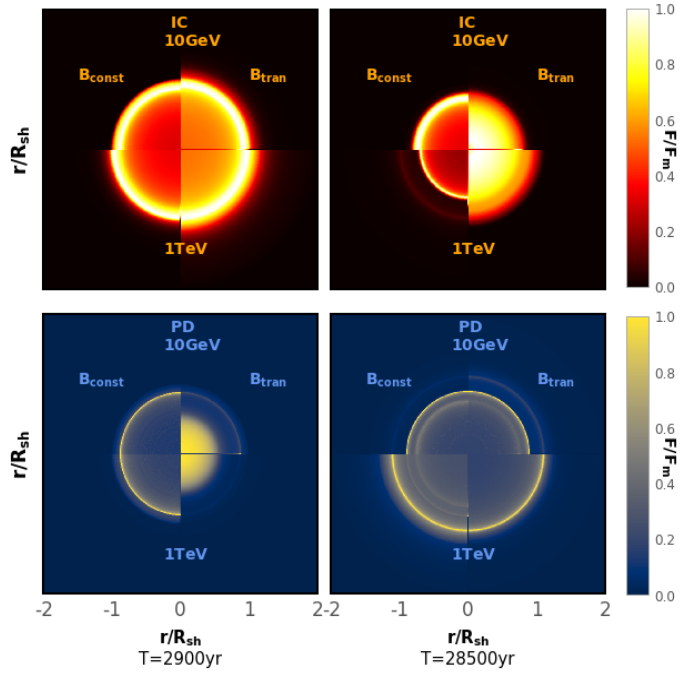

Figure 6: Intensity maps for Inverse Compton (IC) and Pion-Decay (PD) emission from an SNR located at 1000 parsec distance. Each panel of this Figure is divided into 4 regions: the upper half is for energy 10 GeV and the lower half is for energy 1 TeV, while the left half and right half depict the emission for B_{const} and B_{tran}, respectively. For each specific case, we have calculated the intensity, F/F_m, normalised to its peak value, F_m.

pion-decay (PD) radiation at energies 10 GeV and 1 TeV at 2900 year and 28500 year. After 2900 years, the peak IC intensity comes from the electrons at the FS for both B_{const} and B_{tran}. In the B_{tran} scenario, the weaker magnetic field permits electrons to travel further downstream and provide more emission than with B_{const}. PD emission emanates from two regions: dense SNR ejecta and around the contact discontinuity between the FS and reverse shock (RS). For B_{const}, protons are trapped around RS and make that region bright, whereas for B_{tran}, protons accelerated at FS can penetrate deeply into the SNR and illuminate the ejecta region. After 28500 years, the maximum IC intensity emanates from the RS, energised by several reflected shocks for B_{const} and in the B_{tran} framework, IC emission is originated from the entire region inside the RS specifically where the magnetic field is lower. In the PD emission, a shell-like structure is visible at 1 TeV originated at the contact discontinuity between shocked wind and shocked ISM, whereas at 10 GeV, the highest PD intensity comes from the region around the RS and the contact discontinuity between FS and RS.

3. Conclusions

In this work, we have considered a non-rotating $60M_\odot$ progenitor star with solar metallicity which provides spectra softer than E^{-2} spectra as the star creates a hot bubble during its evolution. For comparison, if we consider a $20M_\odot$ progenitor star which evolves only through Main-Sequence and Red-Supergiant stage should not provide spectra as soft as the presented scenario, as most of the bubble would not be hot enough. For a $35M_\odot$ progenitor star, although it becomes Wolf-Rayet star after being a Red-Supergiant, the hydrodynamics would be very different from this discussed work and that will provide different spectral shapes in particle spectra. Therefore, focusing the influence of CSM hydrodynamics and magnetic field, it can be concluded that,

- Constant compressed magnetic field ($B_{\rm const}$) represents the effect of hydrodynamics whereas transported magnetic field ($B_{\rm tran}$) exhibits the consequence of CSM magnetic field on the particle acceleration by constraining the particle diffusion, maximum achievable energies, and finally, to shape the particle spectra.
- Soft cosmic ray spectra must be expected when the SNR shock passes through hot shocked wind. In this presented work, spectral index reaches 2.5 at this specific region.
- The spectral shape depends on the temperature of the bubble, the interactions between FS and structures inside the bubble, and magnetic field. Hence they completely depend on the evolutionary stages of progenitor stars.
- The inverse Compton and pion decay emission reflect the magnetic field structure, distribution of particles, and spectral properties of the particles. The highest intensity can at times be observed in the center and at other times at the rim.

References

[1] M. Cardillo, E. Amato, and P. Blasi *Supernova remnant W44: a case of cosmic-ray reacceleration* A&A, 595:A58 , 2016

[2] M. Pohl, A.Wilhelm, and I.Telezhinsky *Reacceleration of electrons in supernova remnants* A&A, 574:A43, 2015

[3] M. A. Malkov, P. H. Diamond, and R. Z. Sagdeev *Mechanism for spectral break in cosmic ray proton spectrum of supernova remnant W44*, *Nature Communications*, 2, 194, 2011

[4] R. Brose, M. Pohl, I. Sushch, O. Petruk, and T. Kuzyo, *Cosmic-ray acceleration and escape from post-adiabatic supernova remnants* A&A, 634:A59 , 2020

[5] J. H. Groh, G. Meynet, and S. Ekström, and C. Georgy *The evolution of massive stars and their spectra. I. A non-rotating 60 $M_\odot$ star from the zero-age main sequence to the pre-supernova stage* A&A, 564:A30, 2014

[6] S. Ekström, et al. *Grids of stellar models with rotation. I. Models from 0.8 to 120 $M_\odot$ at solar metallicity ($Z = 0.014$)* A&A, 537:A146, 2012

[7] I. Telezhinsky, V. V. Dwarkadas, and M. Pohl *Particle spectra from acceleration at forward and reverse shocks of young Type Ia Supernova Remnants* Astroparticle Physics, 35:300–311, 2012

[8] I. Telezhinsky, V. V. Dwarkadas, and M. Pohl. *Acceleration of cosmic rays by young core-collapse supernova remnants* A&A, 552:A102, 2013

[9] A. Marcowith and F. Casse *Postshock turbulence and diffusive shock acceleration in young supernova remnants* A&A, 515:A90, 2010

[10] P. Blasi, S. Gabici, and G. Vannoni *On the role of injection in kinetic approaches to non-linear particle acceleration at non-relativistic shock waves* MNRAS 361:907-918, 2005

[11] B. K. Shivamoggi *Stellar rotation effects on the stellar winds* Physics of Plasmas 27:012902, 2020

[12] A. Mignone, G.Bodo, S.Massaglia, T. Matsakos, O. Tesileanu, C. Zanni, and A. Ferrari *PLUTO: A Numerical Code for Computational Astrophysics* ApJ 170:228-242, 2007